THE JOURNAL OF PHYSICAL CHEMISTRY A

Article

pubs.acs.org/JPCA

Ab Initio Molecular Dynamics of High-Temperature Unimolecular Dissociation of Gas-Phase RDX and Its Dissociation Products

Igor V. Schweigert*

Code 6189, Theoretical Chemistry Section, US Naval Research Laboratory, 4555 Overlook Ave SW, Washington, D.C. 20375-5342, United States

Supporting Information

ABSTRACT: Unimolecular dynamics of gas-phase hexahydro-1,3,5-trinitro-1,3,5-triazine (RDX) and its dissociation products were simulated using density functional theory (DFT) at the M06-L level. The simulations of RDX at 2000 K showed that dissociation proceeds from multiple conformers, mostly via homolytic fission of an N−N bond with a minor contribution from elimination of HONO, in agreement with previous transition state theory calculations. However, the simulations of the fission and elimination products revealed that secondary N−N fission is facile and, at the simulated temperature of 1750 K, dominant over other mechanisms. The simulations of the resulting intermediates revealed a number of new unimolecular pathways that have not been previously considered. The transition structures and minimal energy paths were calculated for all reactions to confirm these observations. Based on these findings, a revised set of the unimolecular reactions contributing to gas-phase RDX decomposition is proposed.

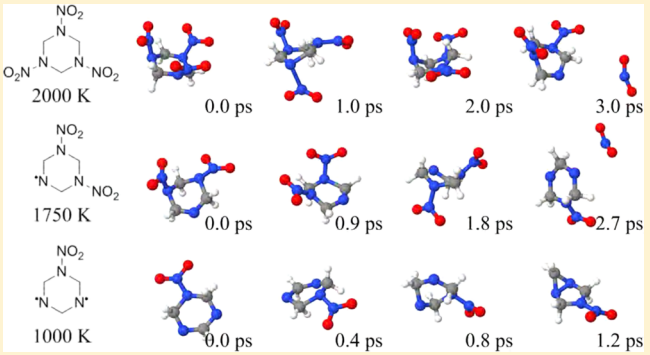

1. INTRODUCTION

A reaction rate model describing decomposition of hexahydro-1,3,5-trinitro-1,3,5-triazine (RDX) at temperatures up to a few thousand kelvin is needed for modeling impact and shock initiation of RDX-based energetic composites. Thermal decomposition of RDX has been subject to a number of experimental studies,[1−16] and the global rates of decomposition for temperatures below 700 K have been derived from the thermogravimetric[9,15] and rapid pyrolysis[10,12] measurements. However, the measured rates cannot be reliably extrapolated to higher temperatures, as global rates approximate complex manifolds of elementary reactions and do not necessarily follow the Arrhenius equation. On the other hand, gas-phase elementary mechanisms have been determined with theoretical calculations,[17−27] and the estimated rate constants[17,24] should be applicable at any temperature. Yet, these calculations have focused on unimolecular and bimolecular pathways that have low activation energies and may have neglected alternative pathways, in which higher activation energies are compensated by higher activation entropies. The objective of this work is to investigate whether temperatures up 2000 K promote new unimolecular pathways that have not been previously considered.

In the gas phase, initial dissociation of RDX proceeds via homolytic fission of N−N bonds or 1,2-elimination of HONO, although concerted fission of multiple C−N bonds, oxygen insertion, and nitro−nitrite isomerization have also been considered as the initial mechanism (Scheme 1). Electronic structure calculations showed that the electronic barriers to N−N fission and HONO elimination are significantly lower than the barriers to the other mechanisms.[17,19,22,23] It remains to be resolved whether fission or elimination has the lowest barrier because the predicted difference is within the accuracy of the *ab initio* methods that have been applied to RDX. However, fission proceeds via a "loose" transition structure (TS) and thus is entropically favored, which is manifested by a large pre-exponential factor in the corresponding rate constant.[24]

Secondary unimolecular reactions of RDX fragments were first discussed by Schroeder,[4] who suggested that the aminyl radical **1a** can undergo ring-opening via C−N β-scission (eq 6, Scheme 2), leading to an acyclic isomer **1b**. He also suggested the possibility of H atom shift (eq 7) leading to a cyclic C-centered radical **1c**. Melius[17] performed empirically corrected many-body perturbation theory calculations on a smaller nitramine and found that the C−N bond dissociation energy in the aminyl radical is indeed significantly lower than in the parent nitramine. He thus confirmed Schroeder's assumption about ring-opening in **1a** leading to **1b** (eq 6). Melius further suggested that another C−N β-scission is facile in **1b** (eq 10), leading to an acyclic N-centered radical **6** and methylenenitramine **MN**. **6** would undergo another C−N β-scission to again yield **MN** (eq 27, Scheme 3), and **MN** can undergo N−N fission or HONO elimination (eqs 32 and 33, Scheme 3). Chakraborty et al.[23] used density functional theory (DFT)

Received: October 3, 2014
Revised: February 27, 2015
Published: March 4, 2015

DOI: 10.1021/jp510034p
J. Phys. Chem. A 2015, 119, 2747−2759

Scheme 1. Unimolecular Reactions of RDX

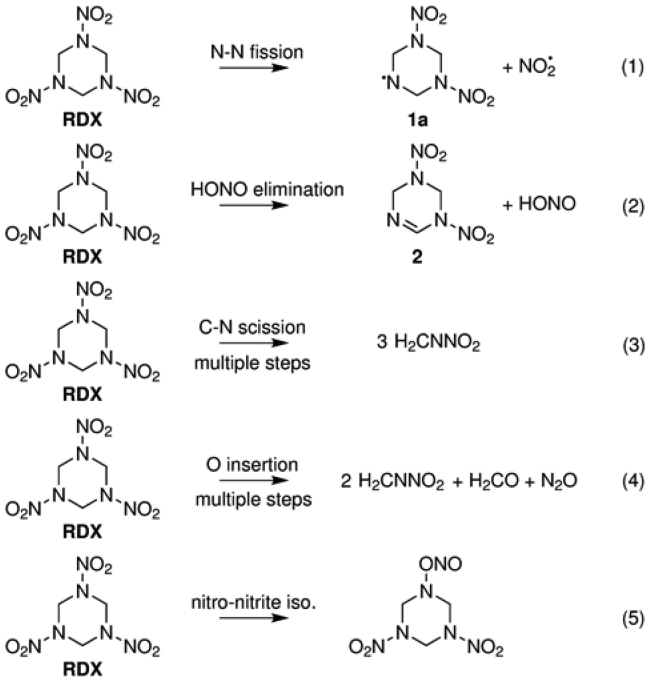

calculations at the B3LYP/6-31G(d) level to verify these mechanisms and to seek other possible pathways. They found that **1b** can also undergo H atom shift (eq 9) to form an acyclic C-centered radical **1d**. They suggested that **1d** can further undergo successive β scission (eqs 13 and 17) to first form **3** and then **9**. They also proposed that the elimination product **2** can undergo successive HONO elimination yielding first **7** (eq 15) and then 1,3,5-triazine **13** (eq 29), and **13** can undergo concerted scission of three C−N bonds yielding HCN (eq 43, Scheme 4). Recently, Irikura[27] used the isopotential search method at a semiempirical level followed by DFT calculations to study unimolecular and bimolecular pathways of RDX decomposition. He confirmed some of the unimolecular pathways of Chakraborty et al. found that 1,4 H shift in **1a** (eq 7) has a lower barrier than 1,2 shift and suggested the possibility of nitro-*aci* isomerization in **1a** and **1b**. To summarize, these studies identified C−N β-scission and H shift as the key secondary mechanisms responsible for unimolecular dissociation of the radical product **1a** of fission in RDX and secondary HONO elimination as the mechanism of unimolecular dissociation of **2**. Reaction rate models that include these mechanisms are available.[17,24]

The present study was initially motivated by the omission of secondary N−N fission in the above studies. N−N fission in **1a** (eq 8) was ruled out in ref 23 because the energy of the cyclic biradical **4a** was deemed to be too high. Instead, a reaction of simultaneous H shift and N−N fission (not shown) was included, despite its barrier being significantly higher than the barrier to N−N fission in RDX. N−N fission in **2** (eq 14) was not considered at all. Our preliminary investigation showed that neither the unpaired electron in **1a** nor the double bond in **2** had a significant effect on the remaining N−N bonds and the electronic barriers to N−N fission in **1a** and **2** were found to be similar to RDX. Further, comparing the Arrhenius parameters from ref 24 shows that, owing to its much larger prefactor, N−N fission in RDX is faster than C−N β-scission in **1a** (eq 9) at temperatures above ∼1200 K, even though the latter has a notably lower activation energy. These findings prompted the present reinvestigation of the secondary unimolecular reactions of RDX fragments.

Scheme 2. Unimolecular Reactions of the Dinitro Intermediates of RDX Dissociation

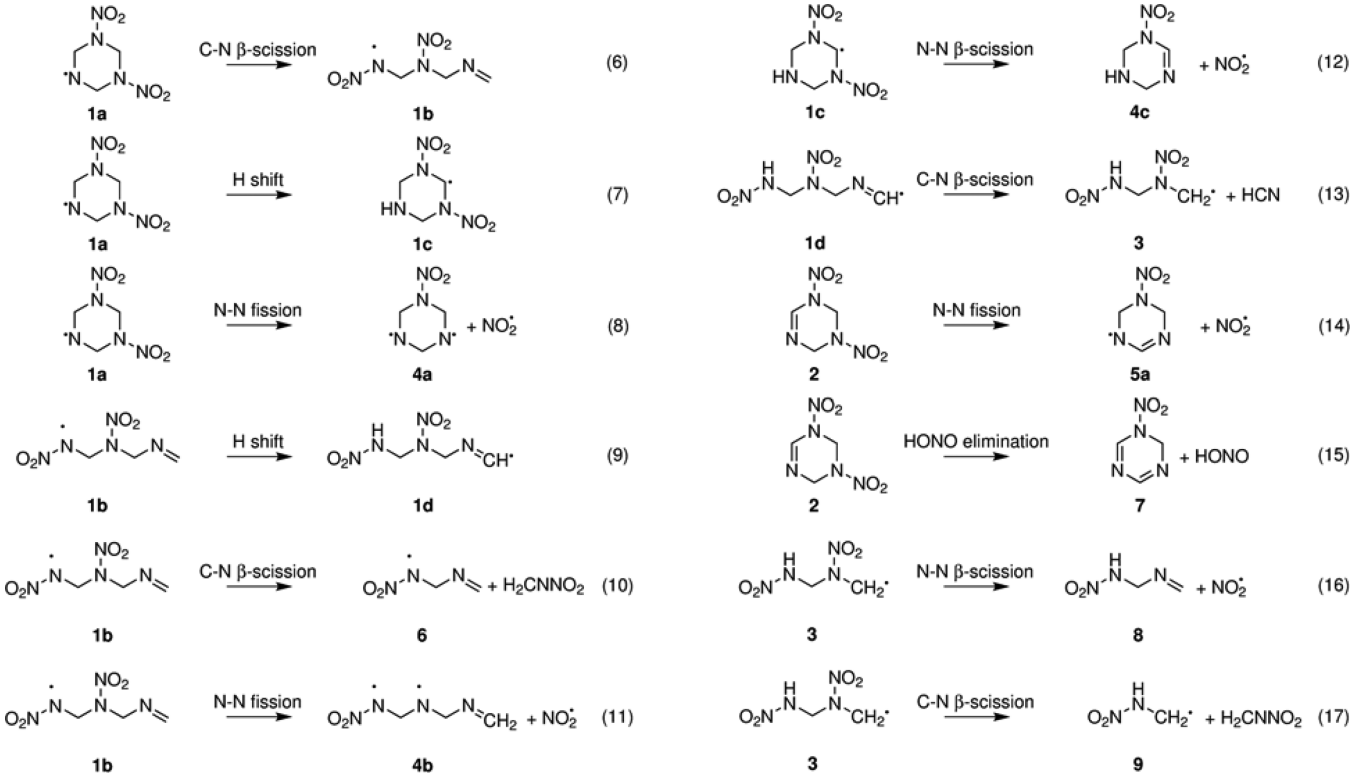

DOI: 10.1021/jp510034p
J. Phys. Chem. A 2015, 119, 2747−2759

Scheme 3. Unimolecular Reactions of the Mononitro Intermediates of RDX Dissociation

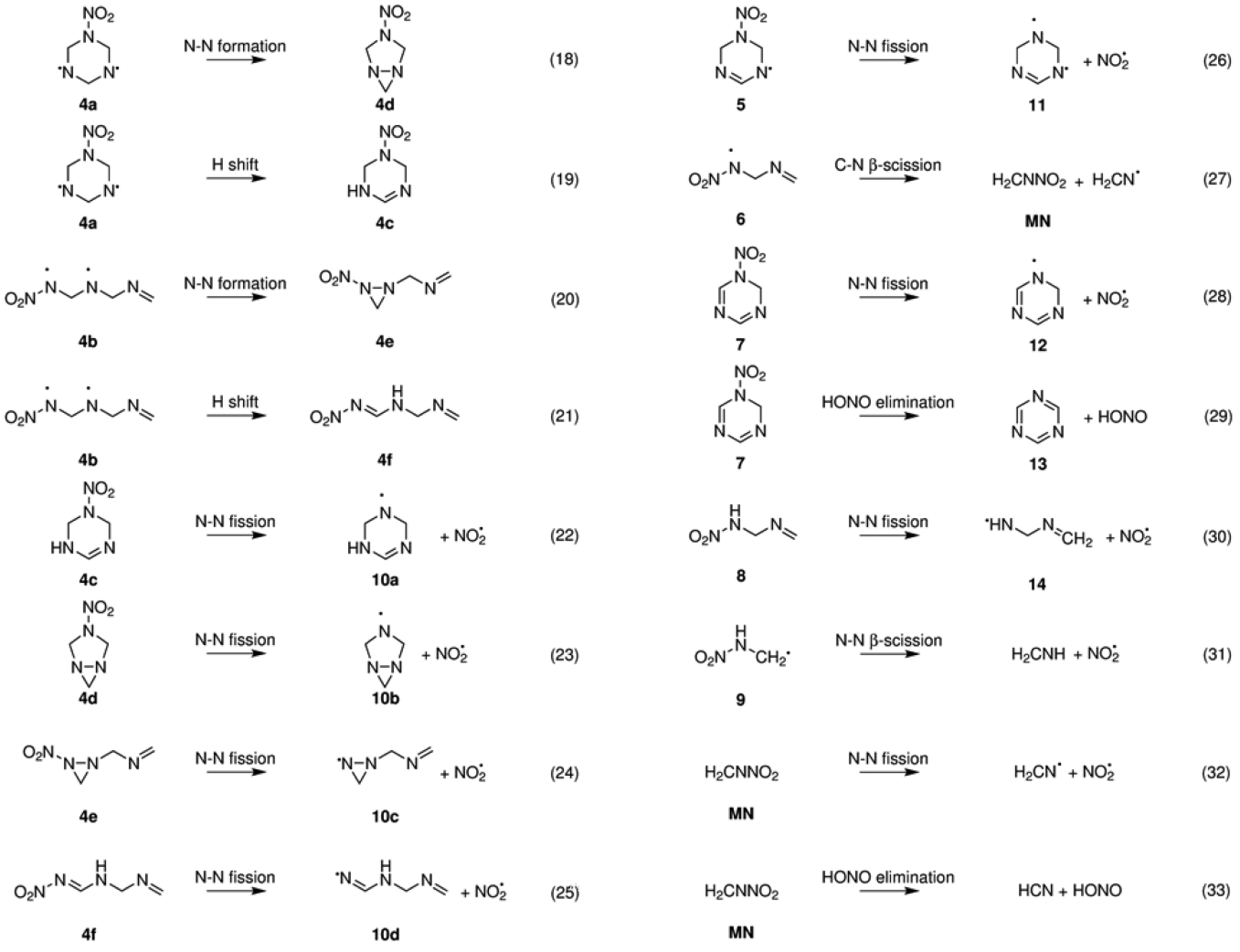

Here, DFT-based *ab initio* molecular dynamics (MD) in its quasiclassical trajectory (QCT) formulation[28−30] was used to simulate the unimolecular reactions of RDX and its dissociation products at temperatures up to 2000 K. The initial atomic coordinates and velocities for each species were sampled using the Boltzmann distribution of the quantized vibrational modes and the ensuing classical dynamics was simulated in the microcanonical (NVE) ensemble. Using the QCT approach eliminated the need for thermostatting and its possible effect on the reactive dynamics. A similar procedure was used by Sewell and Thompson (refs 18 and 11) to study unimolecular dynamics in RDX on a model potential energy surface (PES). Here, DFT was used directly to eliminate the need for an analytical PES. The forces on the nuclei were computed at each MD step using the M06-L density functional,[31] which is based on the meta generalized gradient approximation. Multiple trajectories were computed for each species, starting with RDX and continuing to its dissociation intermediates. The trajectories were analyzed to identify reaction mechanisms. To verify the observed reaction mechanisms, the corresponding transition structures (TS's) were found at the same level of theory, and the minimal-energy paths (MEP's) connecting the reactant to product species were computed using the intrinsic reaction coordinate (IRC) approach.[32,33]

The remainder of the paper is organized as follows. Computational methods are described in detail in section 2. Results are presented and discussed in section 3. Concluding remarks are given in section 4.

2. COMPUTATIONAL METHODS

The MD and IRC calculations were done with the M06-L functional[31] combined with the 6-31+G(d, p) set[34] of Gaussian-type atomic orbitals (GTO's) and the W06 set[35] of GTO's for the variational fitting[36] of the charge density, as implemented in the Gaussian09 code.[37] The unrestricted variant of the Kohn−Sham (KS) equations was used in all calculations. Intersystem crossings and spin-forbidden reaction channels were not considered, and all the species were simulated in their lowest spin state. The orbital stability analysis[38] was performed to ensure that the orbitals (symmetry broken, when appropriate) yielded the lowest-energy KS determinant.

The accuracy of the M06-L functional was tested on several unimolecular reactions in a smaller nitramine **15** and its radical **16** (Scheme 5), similar to those occurring in RDX and **1a**. The M06-L energies along the computed MEP's were compared to coupled-cluster with single and double excitations and the perturbative treatment of triple excitations [CCSD(T)] (see, e.g., ref 39), as implemented in Gaussian09. For N−N fission in

DOI: 10.1021/jp510034p
J. Phys. Chem. A 2015, 119, 2747−2759

Scheme 4. Possible Unimolecular Reactions of 10, 11, 12, 13, and 14

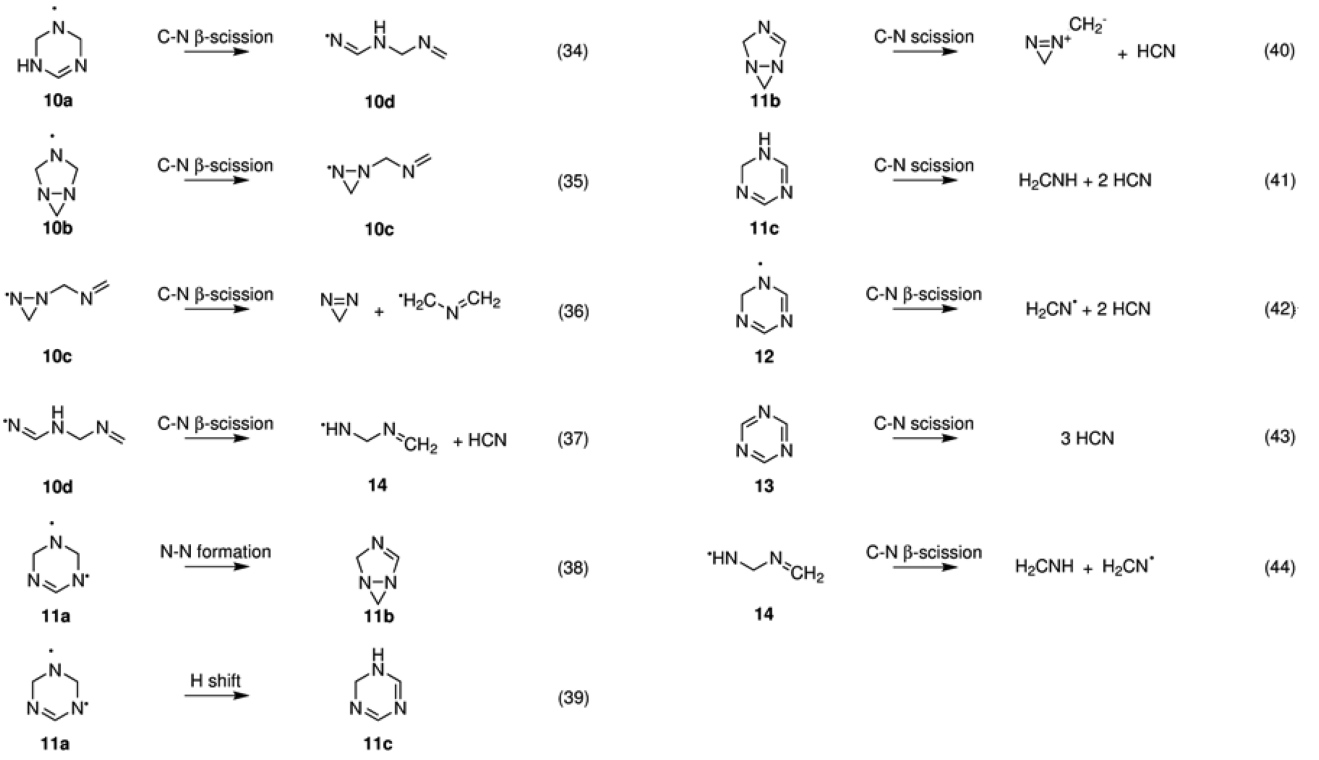

Scheme 5. Unimolecular Reactions of Aminomethylnitramine (15) and Its Radical (16) Used To Test the Accuracy of the M06-L Functional

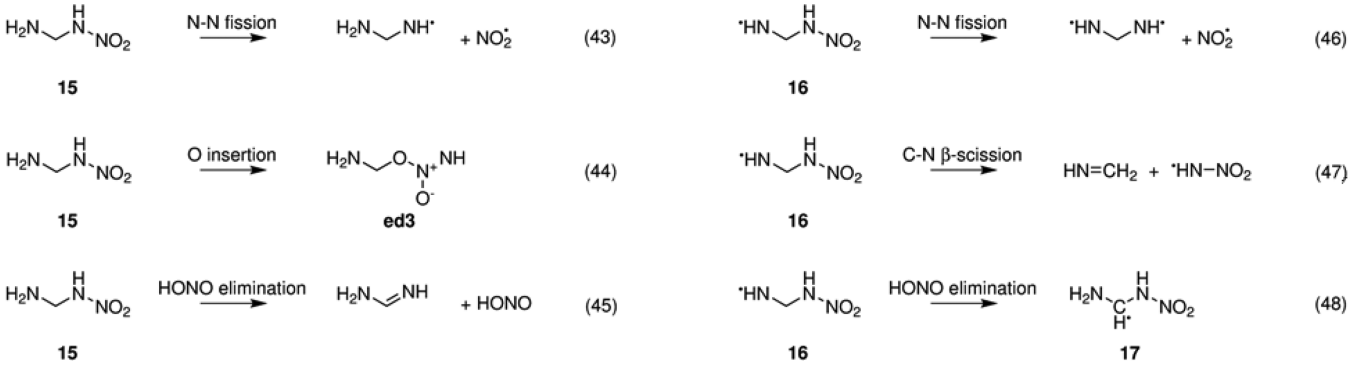

15 and **16**, the energies were also compared to complete active space self-consistent field (CASSCF), as implemented in MOLPRO.[40] The CCSD(T) and CASSCF calculations were done with the aug-cc-pVTZ basis set.[41]

The equilibrium structures of all species were obtained by unconstrained optimization. The Cartesian coordinates for all structures are provided in the Supporting Information. The harmonic vibrational frequencies were computed for each optimized structure to ensure a local minimum was found and to provide the input for the vibrational sampling. Multiple conformers were found for most species, but only one conformer was selected for the subsequent MD simulations. In the MD simulations, the temperatures ranged from 1000 to 2000 K, and the average kinetic energy of a single vibrational mode, 8.3−16.6 kJ/mol, was comparable to the electronic barriers[42] between the conformers. Correspondingly, the vibrational sampling was done for a single conformer, for example, the chair AAA conformer of RDX. At the simulated temperatures, interconversion was assumed to be faster than dissociation, and the MD trajectories were expected to sample reactions from all conformers. As discussed in the next section, this assumption was confirmed for RDX and should hold for the other species.

The vibrational sampling was done using the quasiclassical sampling algorithm of Bunker[43] and Hase,[44] as implemented in Gaussian09. The algorithm randomly assigned a quantum number to each normal mode according to the Boltzmann distribution at the target temperature. The classical amplitudes were computed by equating the classical and quantum energies and combined with randomly selected phases to yield the classical coordinates and momenta in the normal-mode frame. The coordinates were transformed to the molecular frame, thus giving the initial atomic coordinates and velocities. However, the algorithm was found to grossly overestimate the thermal energies of the low-frequency (large-amplitude) vibrational modes, including hindered rotations of the NO_2 groups, ring torsions, and CH_2 wags and twists, for which anharmonicity was expected to be large. This issue was circumvented by

DOI: 10.1021/jp510034p
J. Phys. Chem. A 2015, 119, 2747−2759

excluding any mode below 500 cm^{-1} from the sampling and, instead, assigning it a kinetic energy equal to $2k_bT$.

For each species, 50 sets of the atomic coordinates and velocities were generated using this procedure and used as the initial conditions in the DFT-based microcanonical (NVE) MD simulations. Several microcanonical MD integrators available in Gaussian09 were tested, and the basic velocity Verlet scheme with time step of 0.25 fs was deemed to provide the best combination of stability and computational efficiency. For closed-shell reactants, each trajectory was monitored for an onset of spin polarization and restarted, when necessary,[45] to ensure a seamless transition to the symmetry-broken orbitals. In a few trajectories, the default self-consistent field (SCF) algorithm based on the direct inversion of the iterative subspace[46] was not sufficient to converge the SCF equations along a portion of the trajectory. In these cases, the quadratically convergent SCF algorithm[47,48] was used for a few hundred time steps, and then the simulation was continued with the default algorithm. In most trajectories, the variations in the total energy did not exceed 1 mhartree (~3 kJ/mol). In a few cases, larger energy variations were observed during the postdissociation parts of the trajectories. This did not affect the reaction mechanisms reported below.

Molecular structures from the MD trajectories were saved every 10 fs and analyzed as follows. The interatomic distances between all bonded N−N, C−N, and C−H atoms were computed to check for broken bonds. The distances between all nonbonded O−H and N−H atoms were computed to check for formed bonds. For RDX and **1a**, the time profiles of these distances were plotted to determine the critical distances at which a bond would not revert to its unreacted state and could be considered broken or formed. Extending beyond 3.0 Å was chosen as the criterion for recording a N−N or C−N bond broken and 2.0 Å for a C−H bond. These distances are shorter than the 4.5 Å threshold distances used in ref 18. Reaching 1.0 Å was chosen as the criterion for considering a O−H or N−H bond formed. The structures along the trajectories that satisfied these criteria were saved for subsequent visualization. The reactive trajectories were further propagated until the smallest distance between previously bonded atoms reached 4.0 Å. Visualization of the saved structures showed that, in a few trajectories, breaking of one bond was immediately followed by breaking of another bond, causing the distance analysis to record an incorrect mechanism. The mechanism assignments were checked by comparing the structures extracted from the trajectories to optimized TS's.

Nonreactive trajectories were stopped at 5 ps. This time scale was chosen to allow low-frequency modes (in the terahertz regime) to complete several periods. The chosen cutoff of 5 ps determined the range of the temperatures that can be simulated. For at least 20 out of 50 trajectories to capture a reaction on this time scale, the simulated temperature must be sufficiently high so that the unimolecular rate is on the scale of 10^{11} s^{-1}. Lowering the simulated temperature from 2000 K to, e.g., 1750 K would have required a nearly 5-fold increase in the simulated time to capture a similar number of reactive events. This was deemed impractical: for example, computing 1 ps for RDX on a single Cray XE6 node with 32 cores took about 200 h.

At the target rate of 10^{11} s^{-1}, at least five trajectories were expected to be reactive within the first picosecond. Correspondingly, if fewer than five trajectories were found to be reactive within the first picosecond, the simulations were stopped and the vibrational sampling was redone for a higher temperature. With 5 to 20 trajectories being reactive within the first picosecond, the distribution of reaction lifetimes was found to be comparable to a single-exponential decay. The single-exponential lifetime distributions were interpreted as an indication that the simulated trajectories indeed followed the equilibrium, Rice−Ramsperger−Kassel−Marcus (RRKM) like unimolecular dynamics. On the other hand, notably non-exponential distributions were observed if more than 20 trajectories were reactive within the first picosecond. In these cases, the sampling was redone for a lower temperature.

The TS's for the reactions with an apparent barrier (HONO elimination, β-scission, and H shift) were found using unconstrained optimization. Each such TS had a single imaginary frequency. Approximate TS's for the reactions with no apparent barrier (N−N fission) were found by constrained optimization with the N−N bond length fixed at 3.25 Å. The MEP's connecting reactants, TS's, and products were computed using a Hessian-based predictor−corrector implementation[33,49] of the IRC method.[32] For several reactions, the molecular conformations changed substantially along the MEP's, sometimes connecting the TS to a conformer different from the one used in the vibrational sampling. For these reactions, reasonable effort was made to locate the correct TS conformation, but if not successful, the available conformation was used instead. As a result, some of the MEP's correspond to a conformer different to the one used in the vibrational sampling. Such MEP's have nonzero (but small) ΔE_{elec} at the reactant limit (Figures S4 and S5) because the ΔE_{elec} values were computed with respect to the energy of the conformer used in the sampling.

The thermochemical parameters for all intermediates and TS's were calculated using the ideal gas, rigid rotor, and harmonic oscillator approximations for respectively the translational, rotational, and vibrational partition functions. In these calculations, all vibrational modes were treated as harmonic (no hindered rotor corrections for low-frequency modes) using unscaled frequencies. The electronic barriers ($\Delta E^{\neq}_{elec}$), barriers with vibrational zero-point energy corrections ($\Delta E^{\neq}_{0}$), activation enthalpies ($\Delta H^{\neq}_{298}$), and entropies ($\Delta S^{\neq}_{298}$) at 298 K and 1 bar were computed for each reaction (Table S1, Supporting Information). It should be noted that the activation enthalpies and entropies depend on temperature and for higher temperatures can differ by as much as 10 kJ/mol and 5 J/(mol K) from the computed $\Delta H^{\neq}_{298}$ and $\Delta S^{\neq}_{298}$ values (see Figure S2, Supporting Information). Furthermore, in the case of the N−N fission reactions, the TS's themselves depend on temperature and for higher temperatures would be located at shorter bond lengths than the ones used to estimate the values in Table S1. As a result, the effect of elevated temperatures on the activation enthalpies and entropies of these reactions is more pronounced and the values quoted in Table S1 should be interpreted as approximate upper bounds for the actual values. Altogether, the computed $\Delta H^{\neq}_{298}$ and $\Delta S^{\neq}_{298}$ values are used in the next section only for a qualitative comparison with the MD results. Variational transition-state theory calculations are currently ongoing and should provide quantitative estimates for the corresponding rate constants.

3. RESULTS

Assessment of the M06-L Functional. The accuracy of the MD results reported below directly depends on the accuracy of the PES's calculated with the M06-L functional. This functional is known to generally outperform other

DOI: 10.1021/jp510034p
J. Phys. Chem. A 2015, 119, 2747−2759

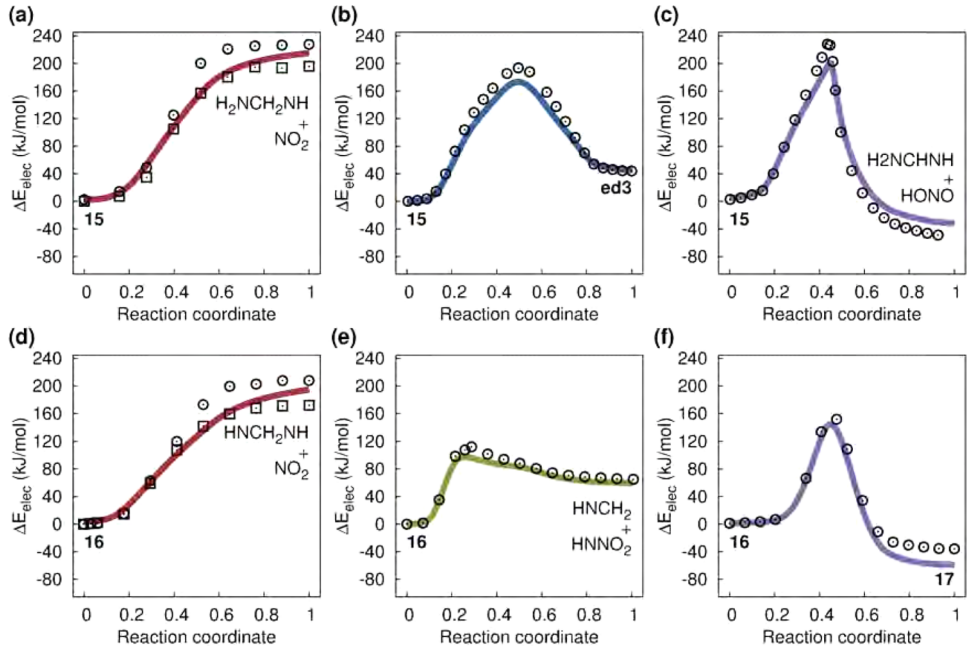

Figure 1. Comparison between the M06-L, CCSD(T), and CASSCF(12e,12o) [(11e,12o) for **16**] energies along the M06-L MEP's for (a) N−N fission, (b) O insertion, (c) HONO elimination in **15**, and (d) N−N fission, (e) C−N β-scission, and (f) H shift in **16**. The M06-L/6-31+G(d,p)/W06 energies are shown with solid lines, the CCSD(T)/aug-cc-pVTZ energies are shown with black circles, and CASSCF(12e/11e,12o)/aug-cc-pVTZ with black squares. All energy values were shifted to match 0 in the reactant limit.

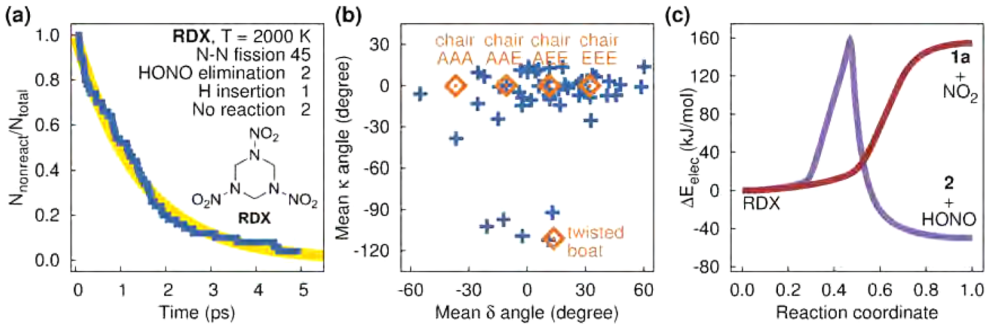

Figure 2. Unimolecular dynamics of RDX at a sampling temperature of 2000 K. (a) The observed reaction lifetimes and mechanisms. Shown in blue is the fraction of the MD trajectories with unreacted molecules as a function of the simulated time. N_{total} = 50. Shown in orange is the corresponding single-exponential fit. (b) The observed RDX conformations just prior to dissociation. Blue crosses show the arithmetic means of the three κ and three δ angles computed for the structures extracted from reactive trajectories wherein one of the N−N bonds lengths first exceeds 3.0 Å or one of the C−H bonds first exceeds 2.0 Å. Orange diamonds show the arithmetic means for the equilibrium structures of the six RDX conformers. (c) Electronic energies along the minimal-energy paths to N−N fission and HONO elimination.

nonhybrid functionals in applications to reaction thermochemistry and activation barriers.[31] Still, several reactions included in Schemes 1, 2, and 3 can be challenging for any level of DFT. For example, homolytic fission in a closed-shell species proceeds via a spin-singlet, open-shell electronic configuration. The accuracy of most density functionals for such a configuration relies on breaking the spin symmetry (i.e., an admixture of the spin-triplet configuration in the KS determinant) and varies depending on the biradical.[50] Homolytic fission in radical species, such as **1a**, proceeds via spin-doublet, open-shell TS, and little is known about how well a symmetry-broken DFT solution approximates the corresponding energy. Also, the electronic barriers to H transfer in the HONO elimination and H shift mechanisms can be underestimated by a nonhybrid functional such as M06-L.

Aminomethylnitramine **15** and its radical **16** (Scheme 5) were selected to test the accuracy of the M06-L energies for a set of reactions similar to those occurring in RDX and **1a**. The TS's to N−N fission, HONO elimination, and O insertion in **15** and N−N fission, H-shift, and C−N β-scission were optimized at the M06-L level and the corresponding MEP's computed. The M06-L and CCSD(T) energies along the MEP's are shown in Figure 1. The CASSCF(12e,12o) energies for N−N fission in **15** and CASSCF(11e,12o) for **16** are also shown. Comparing the electronic energies from the two wave function methods, one should keep in mind that, for homolytic fission, CCSD(T) is expected to underestimate the correlation energy at intermediate values of the reaction coordinate but gives somewhat more accurate energies in the separated-fragment limit.[51] For the TS's O insertion and HONO elimination in **15** and C−N β-scission and H shift in **16**, the CCSD(T) values are expected to be accurate to 10 kJ/mol. Overall, the M06-L energies were found to be within 30 kJ/mol of both wave function methods.

DOI: 10.1021/jp510034p
J. Phys. Chem. A 2015, 119, 2747−2759

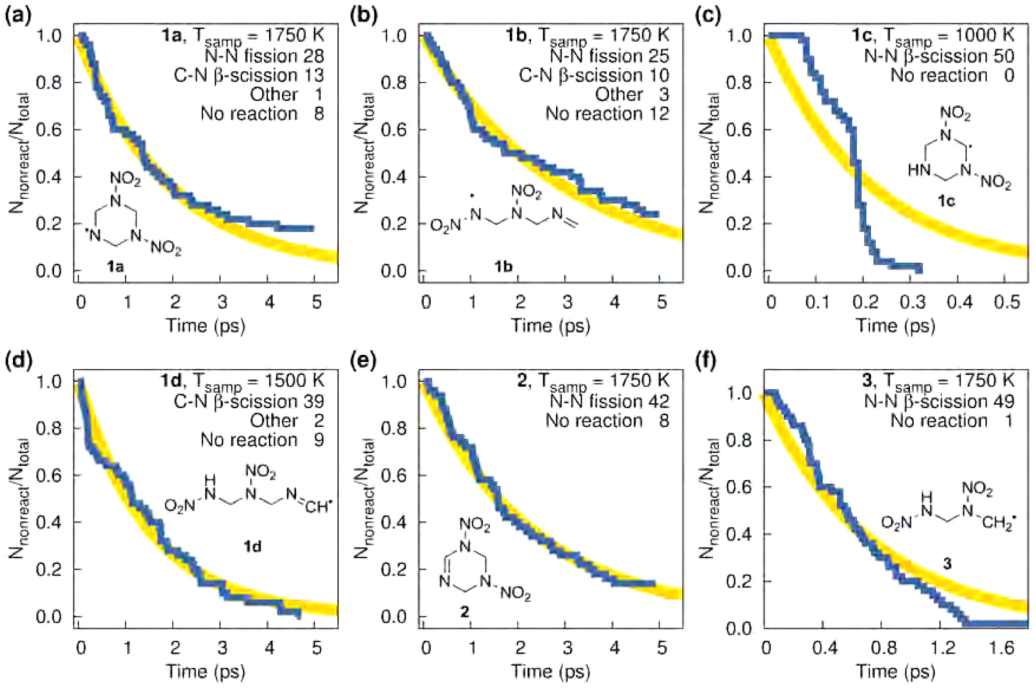

Figure 3. Unimolecular dynamics of the dinitro intermediates at various sampling temperatures (as indicated). See the caption to Figure 2.

Unimolecular Reactions of RDX. In the gas and condensed phases, the RDX molecule is known to adopt several conformations: the triazine ring interconverts between the chair and twisted boat conformations, and the alignments of the N−N bonds can vary from axial (i.e., nearly perpendicular to the ring plane) to equatorial (i.e., nearly parallel to the ring plane).[52,53] The electronic barriers to interconversion were previously estimated to range from a few kJ/mol to about 20 kJ/mol.[42] Six gas-phase conformers reported in ref 52 were optimized at the present level of theory, but no local minimum was found for the boat conformer. The TS's were found to be similar to those reported in ref 42; however, the TS to the twisted boat conformer was found to connect to the chair AAE conformer. The electronic energies along the computed MEP's to interconversion are shown in the Supporting Information (Figure S2a). The κ and δ angles defined in ref 52 were used in the subsequent analysis to differentiate between the conformers (Figure S2b,c).

The unimolecular dynamics of RDX was simulated for a sampling temperature of 2000 K starting with the chair AAA conformer. The observed times to dissociation (reaction lifetimes) and the reaction mechanisms are shown in Figure 2a. Overall, 45 reactive trajectories proceeded via N−N fission, 2 via HONO elimination, and 1 via an unusual mechanism of H insertion into an adjacent C−N bond. Two trajectories remained nonreactive within the total simulated time of 5 ps. No O insertion, concerted C−N scission, or nitro−nitrite rearrangement reactions (Scheme 1) were observed in the simulated dynamics.

The reactive trajectories were analyzed to identify the molecular conformation just prior to dissociation. For each reactive trajectory, the arithmetic means of the κ and δ angles were computed for the structures extracted from the reactive trajectories just prior to dissociation. The observed angles were found to be distributed rather uniformly around the five conformers (Figure 2b). This uniform distribution ascertained that the conformation equilibrium was rapidly established and dissociation proceeded from multiple conformers, even though the sampling was done with the chair AAA conformer.

The TS's to N−N fission and HONO elimination from the chair AAA conformer were found and corresponding MEP's computed. The electronic energies along the MEP's are shown in Figure 2c. In agreement with previous transition state theory calculations,[24] the computed $\Delta H^{\neq}_{298}$ values for the two pathways are similar (Table S1, Supporting Information), but the $\Delta S^{\neq}_{298}$ value for fission is much higher, explaining the branching ratio observed in the MD simulations.

As mentioned above, one MD trajectory captured an H insertion reaction, wherein an elongated C−N bond allowed one of the two adjacent H atoms to bind to the N atom, followed by the loss of the NO_2 group from that N and yielding **1d**. This mechanism resembles the mechanism of simultaneous H shift and N−N fission in **1a** proposed in ref 23. A tight TS to H insertion was found and the IRC calculation (see Figure S3c) showed that, as the H atom binds to the adjacent N atom, the N−N bond in the β-position elongates, resulting in the loss of the NO_2 group and the formation of the acyclic C-centered radical **1d**. The calculated IRC is thus consistent with the observed trajectory. However, the computed $\Delta H^{\neq}_{298}$ and $\Delta S^{\neq}_{298}$ values (Table S1) indicate that the branching ratio for this mechanism is very small. The fact that H insertion was observed despite its negligible branching ratio may indicate a deviation from the RRKM behavior in the simulated dynamics.[54,55] A qualitative comparison of the initial structures, kinetic and potential energies from that specific trajectory, and a few other, randomly selected, trajectories did not reveal any obvious differences. On the other hand, the combined thermal energy of 57 vibrational modes at 2000 K is on the scale of 1000 kJ/mol, and the probability of crossing even a 300 kJ/mol high barrier is finite. The single trajectory showing H insertion was thus classified as an outlier.

To check whether other pathways in Scheme 1 have appreciable branching ratios despite not being observed in the MD simulations, the TS's to O insertion, concerted scission

DOI: 10.1021/jp510034p
J. Phys. Chem. A 2015, 119, 2747−2759

of three C−N bonds, and nitro−nitrite rearrangement were searched for. The TS's to O insertion and C−N scission were found, but the computed $\Delta H^{\neq}_{298}$ and $\Delta S^{\neq}_{298}$ values (Table S1) indicate that the branching ratios for these two mechanisms are an order of magnitude lower than that for HONO elimination. Furthermore, in both cases, the IRC calculations yielded high-energy unimolecular educts (labeled as **ed1** and **ed2** in Figure S3, Supporting Information). Unconstrained optimization confirmed that both educts are local minima with no imaginary frequencies. PES scans (Figure S3, Supporting Information) suggested that **ed1** can undergo C−N fission leading to the loss of a N_2O moiety with $\Delta E^{\neq}_{elec}$ of approximately 70 kJ/mol and then concerted fission of the two remaining C−N bonds leading $2H_2CNNO_2 + H_2CO + N_2O$. **ed2** is a complex of three methylenenitramine (H_2CNNO_2) molecules with an electronic binding energy of approximately 80 kJ/mol. The presence of the educts and multiple barriers makes the reverse reactions facile and should further reduce the branching ratios for these pathways.

A TS for nitro−nitrite isomerization was not found. Several candidate structures were identified, including a loose structure reminiscent of the roaming-radical TS in H_2NNO_2[56] and a tight three-atom structure similar to the TS reported for nitrobenzene.[57] However, the subsequent IRC calculations failed to connect any of these structures to either the nitro or nitrite isomer. The PES scans probing different orientations of the NO_2 group near the radical N reproduced either N−N fission in the nitro isomer or H abstraction by the N atom of the NO_2 group. A detailed study of nitro−nitrite isomerization in smaller nitramines, H_2CNNO_2 and $(CH_3)_2NNO_2$, is ongoing.

Unimolecular Reactions of the Dinitro Intermediates. The unimolecular dynamics of the dinitro dissociation intermediates (Scheme 2) was studied at various sampling temperatures. The results are summarized in Figure 3.

The unimolecular dynamics of the cyclic radical **1a**, starting with its "half-chair" AE conformer, was initially simulated at 2000 K, but the resulting lifetime distribution significantly deviated from a single exponential. The temperature was subsequently lowered, and the results for 1750 K are shown in Figure 3a. Twenty-eight reactive trajectories proceeded via N−N fission, 13 via C−N fission, 1 via HONO elimination, and 8 trajectories remained nonreactive within the simulated time. The observed 2:1 branching ratio of N−N fission to C−N β-scission suggests that secondary N−N fission is not only facile, it is dominant at this temperature. No trajectories showed H shift or nitro-*aci* isomerization.

The TS's for N−N fission and C−N β-scission were found for the "half-chair" AE conformer and the corresponding MEP's computed (Figure S5, Supporting Information). TS's to HONO elimination and nitro-*aci* isomerization were searched for, but the search was not immediately successful and was not pursued further. The electronic barrier to N−N fission in **1a** was found to be nearly identical to that in RDX (Table S1, Supporting Information), confirming our assumption that an unpaired electron on one of the ring N atoms has an insignificant effect on the remaining N−N bonds. The computed $\Delta H^{\neq}_{298}$ and $\Delta S^{\neq}_{298}$ values (Table S1) indicate that while the barrier to N−N fission is notably higher than that to C−N β-scission, the colossal activation entropy of fission should explain the observed 2:1 branching ratio at 1750 K.

The unimolecular dynamics of the acyclic isomer **1b** was simulated for a sampling temperature of 1750 K (Figure 3b), starting with the "broken ring" AA conformer. Twenty-five reactive trajectories proceeded via N−N fission, 10 via C−N β-scission, 1 trajectory via HONO elimination, 1 via C−N bond formation (i.e., the reverse reaction of C−N β-scission in **1a**), 1 via H shift to form **1d**, and 12 trajectories remained nonreactive. One nonreactive trajectory revealed H shift from the α-C atom to an O atom, resulting in a short-lived *aci* tautomer that rapidly undergone a reverse shift back to **1b**. Similar to **1a**, the observed 2.5:1 branching ratio of N−N fission to C−N β-scission suggests that secondary N−N fission in **1b** is facile. The TS's to N−N fission from the α and γ N's, C−N β-scission, and H shift were found for the "broken ring" conformer of **1b**. Note that the computed $\Delta H^{\neq}_{298}$ and $\Delta S^{\neq}_{298}$ values indicate that the branching ratio for H shift should be similar to C−N β-scission. However, H shift is not possible in other conformers of **1b**, wherein the terminal methylene group and the α N are far from each other. Therefore, the branching ratio for H shift, unlike other mechanisms, is strongly affected by the equilibrium distribution among possible conformers of **1b**.

The results of the MD and IRC calculations for **1a** indicate that it is unlikely that the C-centered cyclic isomer **1c** is formed during RDX decomposition because N−N fission and C−N β-scission in **1a** are entropically and energetically favored over H shift. Nevertheless, the simulations of its unimolecular dynamics at 1000 K showed that it undergoes rapid N−N β-scission (Figure 3c). A low-barrier, but well-defined TS to N−N β-scission was found.

The unimolecular dynamics of the acyclic C-centered radical **1d** was simulated at 1500 K (Figure 3d). Thirty-nine reactive trajectories proceeded via C−N β-scission, 2 via N−N fission, and 9 remained nonreactive. The TS to C−N β-scission was found for the trans conformer and the computed $\Delta H^{\neq}_{298}$ and $\Delta S^{\neq}_{298}$ values indicate that C−N β-scission is more facile in **1d** than in **1a** or **1b**, confirming the higher rate of decomposition observed in the MD simulations. Attempts to locate a TS to N−N fission resulted in the NO_2 group "hopping" from the N atom to the radical C atom. In view of the low branching ratio observed in the MD simulations, this mechanism was not studied further.

The unimolecular dynamics of the cyclic intermediate **2** resulting from HONO elimination in RDX was simulated for a sampling temperature of 1750 K (Figure 3e). Forty-two trajectories proceed via N−N fission, and 8 remained nonreactive within the simulated time. No secondary HONO elimination was observed in these simulations. The TS's to fission and elimination were found for the "half-chair" AE conformer, and the computed $\Delta H^{\neq}_{298}$ and $\Delta S^{\neq}_{298}$ values indicate that fission is both *energetically and entropically* favored over elimination. Note that secondary HONO elimination was previously considered[23] to be the only mechanism of **2** dissociation. The present results indicate that the double bond in **2** lowers the barrier to fission while increases the barrier to elimination.

The unimolecular dynamics of the acyclic C-centered radical **3** resulting from C−N β-scission in **1d** was simulated for a sampling temperature of 1000 K (Figure 3e). All trajectories proceeded via N−N β-scission. No C−N β-scission was observed. Note that C−N β-scission was previously considered as the only mechanism.[17,24] The TS's to both N−N and C−N β-scission were found for the trans conformer. The computed $\Delta H^{\neq}_{298}$ and $\Delta S^{\neq}_{298}$ values (Table S1) indicate that N−N β-scission is energetically favored, while the difference in the activation entropies is probably not sufficient for C−N β-

DOI: 10.1021/jp510034p
J. Phys. Chem. A 2015, 119, 2747−2759

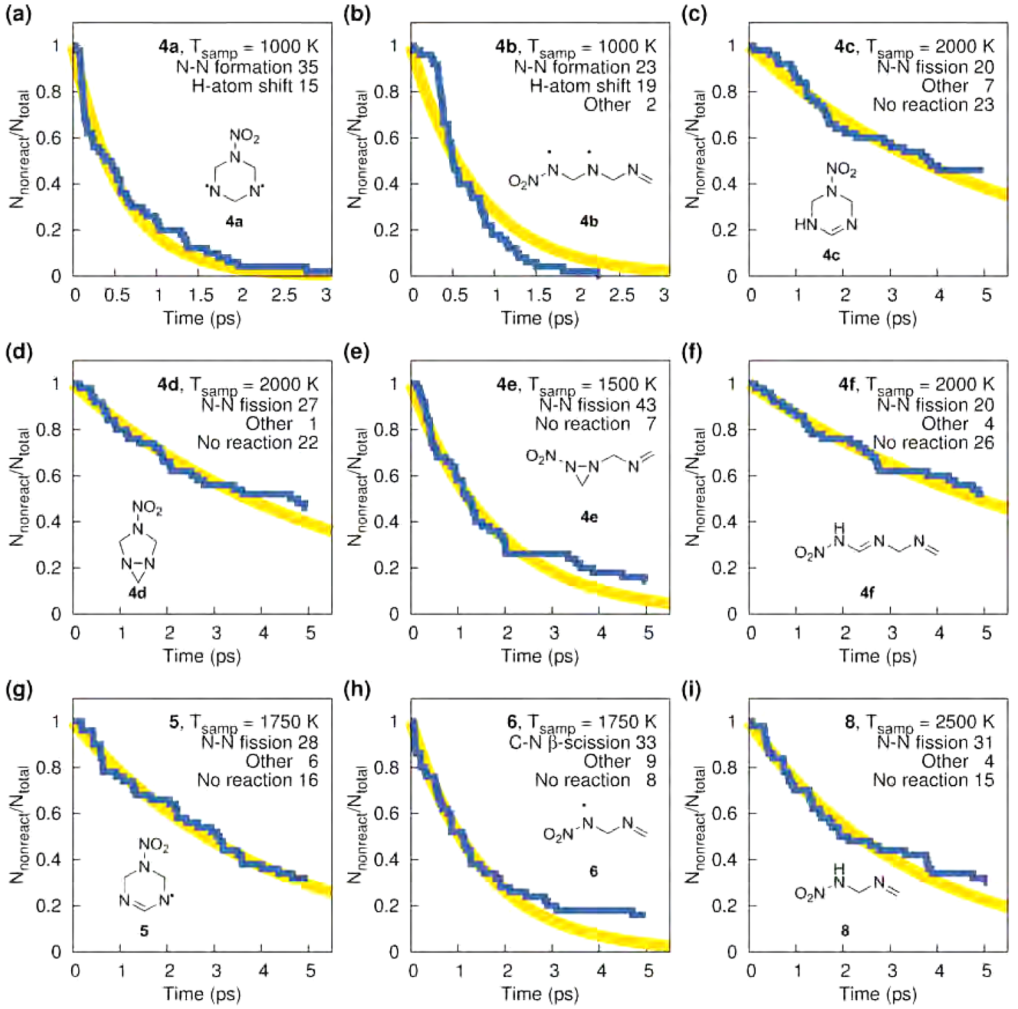

Figure 4. Unimolecular dynamics of the mononitro intermediates at various sampling temperatures (as indicated). See the caption to Figure 2 for details.

scission to have an appreciable branching ratio even at high temperatures.

Unimolecular Dynamics of the Mononitro Intermediates. The unimolecular dynamics of the mononitro dissociation intermediates (Scheme 3) were studied for various temperatures (Figure 4). The intermediates studied were the **4a** and **4b** biradicals resulting from N−N fission in **1a** and **1b**; their closed-shell isomers **4c**, **4d**, **4e**, and **4f** resulting from N−N bond formation and H shift in **4a** and **4b**; the cyclic radical **5a** resulting from N−N fission in **2**; the acyclic radical **6** resulting from C−N β-scission in **1b**; and the closed-shell intermediate **8** resulting from N−N β-scission in **3**. The results of these simulations are summarized in Figure 4.

The unimolecular dynamics of the two biradical intermediates, **4a** and **4b**, was simulated for a sampling temperature of 1000 K (Figure 4a,b). Both biradicals were found to rapidly isomerize to their closed-shell isomers **4c**, **4d**, **4e**, and **4f** via either N−N bond formation or H shift. The computed $\Delta H^{\neq}_{298}$ and $\Delta S^{\neq}_{298}$ values indicate that the higher barriers to H shift are compensated by the higher activation entropies, thus confirming the branching ratios observed in the MD simulations. Note also that N−N fission was observed in two reactive trajectories of **4b** (labeled as "Other" in Figure 4), but the branching ratio was deemed to be too low to warrant searching for the corresponding TS.

The unimolecular dynamics of the closed-shell intermediates **4c**, **4d**, **4e**, and **4f** were simulated for various sampling temperatures (Figure 4c−f). In each case, the dominant mechanism was N−N fission leading to four different isomers of the $C_3H_6N_3$ radical (**10**). However, **4e** was found to be much more reactive with the reaction lifetime at 1500 K being similar to the reactions lifetimes of **4b**, **4c**, and **4d** at 2000 K. The computed $\Delta H^{\neq}_{298}$ and $\Delta S^{\neq}_{298}$ values confirm that the barrier to N−N fission in **4e** is much lower than that in **4c**, **4d**, and **4f**. Also, in the MD simulations of **4c**, **4d**, and **4f**, some trajectories showed C−N fission, but the branching ratios were deemed to be too low to warrant searching for the corresponding TS's.

The unimolecular dynamics of the cyclic radical intermediate **5** was simulated for a sampling temperature of 1750 K (Figure 4g). Similar to the cyclic radical **1a**, **5** was found to undergo N−N fission leading to a cyclic biradical, **11**. The computed $\Delta H^{\neq}_{298}$ and $\Delta S^{\neq}_{298}$ values were found to be similar to that for N−N fission in **1a** (Supporting Information). A few trajectories showed C−N β-scission leading to an acyclic radical isomer resembling **1b**. However, PES scans indicated an electronic barrier higher than N−N fission, and this mechanism was not considered further.

The unimolecular dynamics of the acyclic radical intermediate **6** resulting from C−N β-scission in **1b** was simulated for a sampling temperature of 1750 K (Figure 4h). Thirty-three

DOI: 10.1021/jp510034p
J. Phys. Chem. A 2015, 119, 2747−2759

Scheme 6. Unimolecular Reactions Contributing to Gas-Phase RDX Decomposition[a]

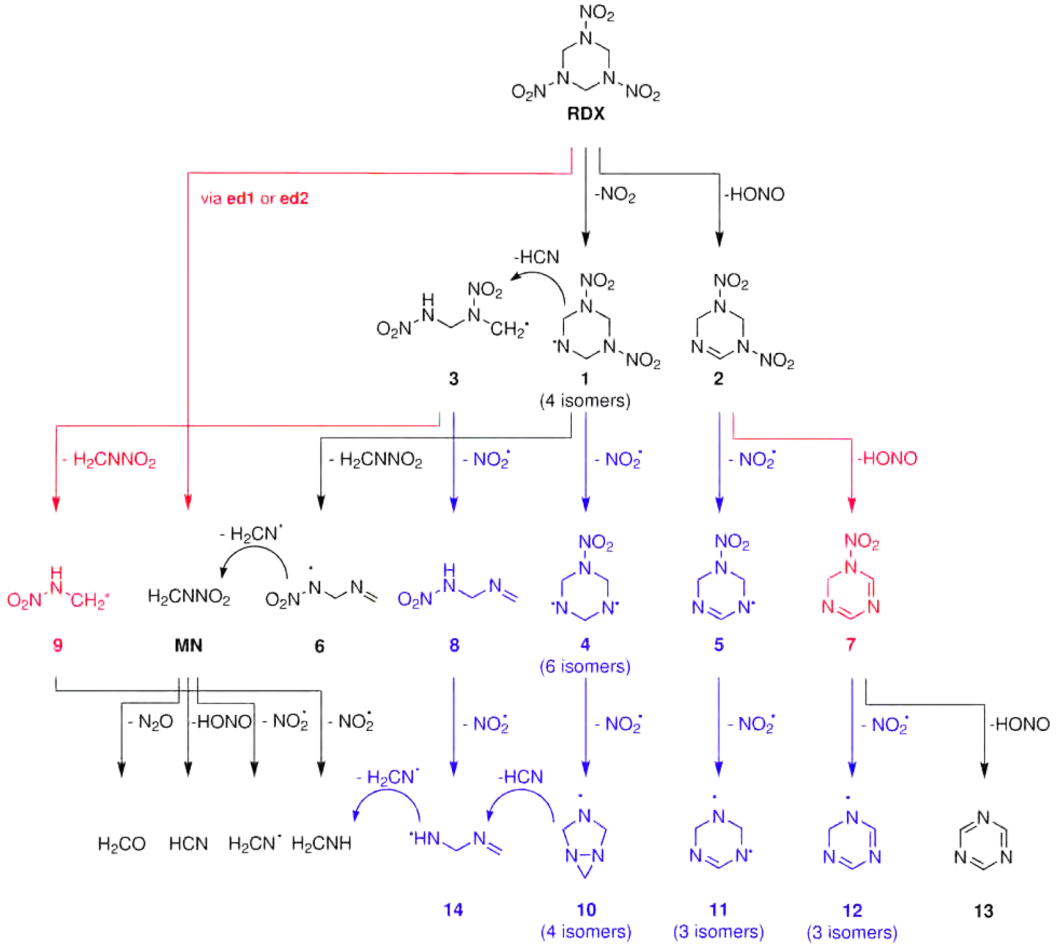

[a]Reactions shown in black were previously known and are confirmed by the present simulations. Reactions shown in blue have not been previously considered but are observed in the present MD simulations. Reactions shown in red were previously known, but the present simulations suggest alternative pathways.

reactive trajectories proceeded via C−N β-scission leading to H_2CNNO_2 and H_2CN. The subsequent TS and IRC calculations revealed a loose TS with a low electronic barrier, in agreement with previous calculations.[23] Nine reactive trajectories revealed N−N fission, but searching for the corresponding TS was not immediately successfully and was not pursued further.

The unimolecular dynamics of the cyclic intermediate **7** resulting from HONO elimination in **2** was not simulated because N−N fission in **2** was found to be both energetically and entropically favored over elimination. Nevertheless, the TS's to N−N fission and HONO elimination in **7** were found and the computed $\Delta H^{\neq}_{298}$ and $\Delta S^{\neq}_{298}$ values are shown in Table S1.

The unimolecular dynamics of the acyclic closed-shell intermediate **8** was simulated for various sampling temperatures. The rate of its dissociation was found to be too low for all but 2500 K (Figure 4i). At this sampling temperature, 31 reactive trajectories proceeded via N−N fission leading to **12** and NO_2, 4 via other mechanisms, and 15 trajectories remained unreacted. The TS to N−N fission was found to have the highest barrier among all N−N fission reactions considered here (Table S1, Supporting Information), thus confirming the relatively low rate of unimolecular dissociation observed in the MD simulations.

The unimolecular dynamics of the acyclic radical intermediate **9** resulting from C−N β-scission in **3** was not simulated because it was not observed in the MD simulation and the computed $\Delta H^{\neq}_{298}$ and $\Delta S^{\neq}_{298}$ values for N−N β-scission in **3** indicated that its favored over C−N β-scission. Like the two other C-centered radicals, **1c** and **3**, N−N β-scission should be facile in **9**, and indeed a low-energy TS to N−N β-scission was found.

Possible Unimolecular Reactions of Other Intermediates. The unimolecular dynamics of **10**, **11**, **12**, **13**, and **14** were not studied, but possible unimolecular mechanisms are suggested in Scheme 4. By analogy with **1a** and **1b**, H shift and β-scission of C−N bonds seem to be the only plausible unimolecular pathways for the radical intermediates **10a**−**10c**, **12** and **14**, since they have no NO_2 moiety. The transition structures for these pathways were found, and the computed $\Delta H^{\neq}_{298}$ and $\Delta S^{\neq}_{298}$ values indicate that β-scission is both energetically and entropically favored (Table S2, Supporting Information). Further, by analogy with **4a**, **11a** is expected to isomerize via N−N formation or H shift to yield two closed-shell isomers, **11b** and **11c**. Concerted scission of multiple C−N bonds seems to be the only plausible unimolecular pathway for **11b** and **11c** as well as **13**. However, the computed $\Delta H^{\neq}_{298}$ and $\Delta S^{\neq}_{298}$ values indicate that these intermediates have very low rates of unimolecular dissociation (Table S2, Supporting

DOI: 10.1021/jp510034p
J. Phys. Chem. A 2015, 119, 2747−2759

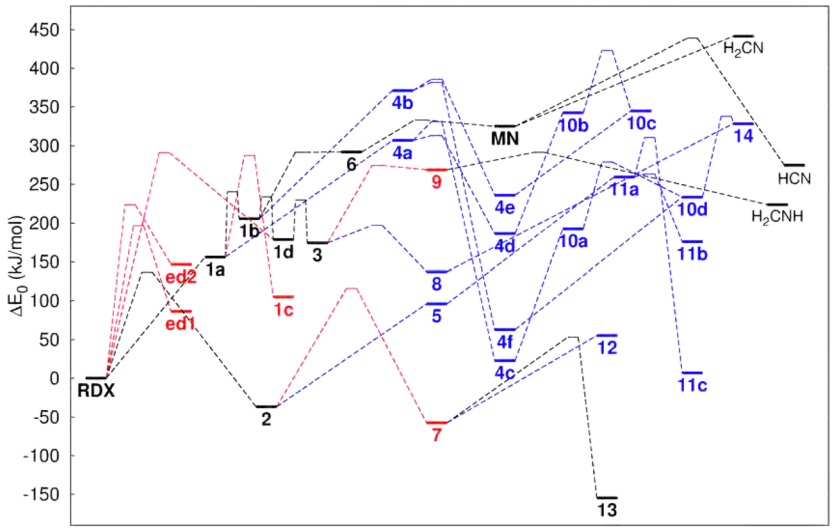

Figure 5. Electronic energies with zero-point-energy corrections of all the intermediate species and transition structures studied in this work. Each value shown corresponds to the total energy of the intermediate indicated by the label and the complementary fragments relative to RDX.

Information). It should be noted that by the time these intermediates are formed, the concentration of radical by-products is large and bimolecular reactions should be facile.

4. SUMMARY

The presented MD and IRC simulations revealed several new unimolecular reaction pathways in gas-phase RDX decomposition. Secondary N−N fission was found to be facile in **1a** and **1b** and dominant over C−N β-scission and H shift at the simulated temperatures. The resulting biradicals **4a** and **4b** rapidly isomerized via N−N formation or H shift, and their closed-shell isomers **4c**, **4d**, **4e**, and **4f** undergone tertiary N−N fission. N−N fission was found to be more facile than HONO elimination in **2**. N−N β-scission was found to be more facile than C−N β-scission in **3**, and N−N fission was found to be the only unimolecular mechanism in the resulting mononitro intermediate **8**. A revised set of unimolecular pathways that incorporates these findings is shown in Scheme 6. The electronic energies with zero-point-energy corrections for all intermediates and TS's are shown in Figure 5. As discussed above, the new N−N fission pathways are expected to become dominant above 1250 K. N−N fission in **2** and N−N β-scission in **3** are expected to dominate over respectively HONO elimination and C−N β-scission at all temperatures. Transition state theory calculations are under way to provide the Arrhenius parameters for the corresponding rate constants.

The full reaction network responsible for gas-phase RDX decomposition is far from being completed understood. The results presented here revealed new unimolecular mechanisms that should be added to the available models. Bimolecular reactions among RDX, its molecular fragments, and the small radicals[17,25,27] are likely to compete with the unimolecular reactions included in Scheme 6. At the same time, it is difficult (if at all possible) to *a priori* rule out a particular class of reactions. Interactions between various elementary mechanisms may lead to kinetic bottlenecks[58] or autocatalytic cycles.[17,27] Such a complexity is well-known in hydrocarbon combustion.[59] There, a commonly accepted approach is to include all known elementary reactions into a detailed "master" mechanism. The detailed mechanism can then be reduced, under specific thermodynamic conditions of interest, to a few-step rate model[60−62] that is suitable for material modeling.[63−71] A validated gas-phase mechanism can also serve as a stepping stone toward understanding elementary decomposition reactions in the condensed phases.

■ ASSOCIATED CONTENT

Supporting Information

Computed $\Delta H^{\neq}_{298}$ and $\Delta S^{\neq}_{298}$ values for reactions 1−39, the minimal energy paths describing unimolecular dissociation of **ed1**, **ed2**, **1a**−**1d**, **2**, **3**, **4a**−**4f**, **5**, **6**, and **8**, and the Cartesian coordinates of all the intermediates and transition structures. This material is available free of charge via the Internet at http://pubs.acs.org.

■ AUTHOR INFORMATION

Corresponding Author

*Phone +1-202-767-2160; Fax +1-202-404-1838; e-mail igor.schweigert@nrl.navy.mil.

Notes

The authors declare no competing financial interest.

■ ACKNOWLEDGMENTS

The author thanks the anonymous reviewers for critical comments, which were helpful in revising the manuscript. This work was supported by the Office of Naval Research, both directly and through the Naval Research Laboratory, and by the Department of Defense High Performance Computing Modernization Program Software Application Institute for Multiscale Reactive Modeling of Insensitive Munitions.

■ REFERENCES

(1) Robertson, A. J. B. The Thermal Decomposition of Explosives. 2. Cyclotrimethylenetrinitramine and Cyclotetramethylenetetranitramine. *Trans. Faraday Soc.* **1949**, *45*, 85−93.

(2) Rauch, F. C.; Fanelli, A. J. Thermal Decomposition Kinetics of Hexahydro-1,3,5-Trinitro-S-Triazine above Melting Point - Evidence for Both a Gas and Liquid Phase Decomposition. *J. Phys. Chem.* **1969**, *73*, 1604.

(3) Cosgrove, J. D.; Owen, A. J. Thermal Decomposition of 1,3,5-Trinitro Hexahydro-1,3,5-Triazine (RDX). 1. Products and Physical Parameters. *Combust. Flame* **1974**, *22*, 13.

DOI: 10.1021/jp510034p
J. Phys. Chem. A 2015, 119, 2747−2759

(4) Schroeder, M. A. *Critical Analysis of Nitramine Decomposition Data: Activation Energies and Frequency Factors for HMX and RDX Decomposition*, 1985.
(5) Oyumi, Y.; Brill, T. B. Thermal-Decomposition of Energetic Materials. 3. A High-Rate, In situ, FTIR Study of the Thermolysis of RDX and HMX with Pressure and Heating Rate as Variables. *Combust. Flame* **1985**, *62*, 213−224.
(6) Oyumi, Y.; Brill, T. B. Thermal-Decomposition of Energetic Materials. 22. The Contrasting Effects of Pressure on the High-Rate Thermolysis of 34 Energetic Compounds. *Combust. Flame* **1987**, *68*, 209−216.
(7) Zuckermann, H.; Greenblatt, G. D.; Haas, Y. Hydroxyl Radical Formation in the Infrared Multiphoton Decomposition of Jet-Cooled Cyclic Nitroamines. *J. Phys. Chem.* **1987**, *91*, 5159−5161.
(8) Zhao, X.; Hintsa, E. J.; Lee, Y. T. Infrared Multiphoton Dissociation of RDX in a Molecular Beam. *J. Chem. Phys.* **1988**, *88*, 801−810.
(9) Behrens, R.; Bulusu, S. Thermal Decomposition of Energetic Materials. 4. Deuterium-Isotope Effects and Isotopic Scrambling (H/D, C-13/O-18, N-14/N-15) in Condensed-Phase Decomposition of 1,3,5-trinitrohexahydro-s-triazine. *J. Phys. Chem.* **1992**, *96*, 8891−8897.
(10) Brill, T. B.; Brush, P. J.; Kinloch, S. A.; Gray, P. Condensed Phase Chemistry of Explosives and Propellants at High-Temperature - HMX, RDX and BAMO. *Philos. Trans. R. Soc. London, A* **1992**, *339*, 377−385.
(11) Chambers, C. C.; Thompson, D. L. Further-Studies of the Classical Dynamics of the Unimolecular Dissociation of RDX. *J. Phys. Chem.* **1995**, *99*, 15881−15889.
(12) Thynell, S. T.; Gongwer, P. E.; Brill, T. B. Condensed-Phase Kinetics of Cyclotrimethylenetrinitramine by Modeling the T-Jump/Infrared Spectroscopy Experiment. *J. Propul. Power* **1996**, *12*, 933−939.
(13) Gongwer, P. E.; Brill, T. B. Thermal Decomposition of Energetic Materials 73: The Identity and Temperature Dependence of "Minor" Products from Flash-Heated RDX. *Combust. Flame* **1998**, *115*, 417−423.
(14) Shu, Y.; Korsounskii, B. L.; Nazin, G. M. Mechanism of Thermal Decomposition of Secondary Nitramines. *Russ. Chem. Rev.* **2004**, *73*, 293−307.
(15) Maharrey, S.; Behrens, R. Thermal Decomposition of Energetic Materials. 5. Reaction Processes of 1,3,5-Trinitrohexahydro-s-triazine below Its Melting Point. *J. Phys. Chem. A* **2005**, *109*, 11236−11249.
(16) Patterson, J. E.; Dreger, Z. A.; Miao, M. S.; Gupta, Y. M. Shock Wave Induced Decomposition of RDX: Time-Resolved Spectroscopy. *J. Phys. Chem. A* **2008**, *112*, 7374−7382.
(17) Melius, C. F. In *Chemistry and Physics of Energetic Materials*; Bulusu, S. N., Ed.; Kluwer: Dordrecht, 1990.
(18) Sewell, T. D.; Thompson, D. L. Classical Dynamics Study of Unimolecular Dissociation of Hexahydro-1,3,5-Trinitro-1,3,5-Triazine (RDX). *J. Phys. Chem.* **1991**, *95*, 6228−6242.
(19) Habibollahzadeh, D.; Grodzicki, M.; Seminario, J. M.; Politzer, P. Computational Study of the Concerted Gas-Phase Triple Dissociations of 1,3,5-Triazacyclohexane and Its 1,3,5-Trinitro Derivative (RDX). *J. Phys. Chem.* **1991**, *95*, 7699−7702.
(20) Sewell, T. D.; Chambers, C. C.; Thompson, D. L.; Levine, R. D. Power Spectral Study of the Classical Vibrational Dynamics of RDX. *Chem. Phys. Lett.* **1993**, *208*, 125−134.
(21) Harris, N. J.; Lammertsma, K. Ab initio Density Functional Computations of Conformations and Bond Dissociation Energies for Hexahydro-1,3,5-trinitro-1,3,5-triazine. *J. Am. Chem. Soc.* **1997**, *119*, 6583−6589.
(22) Wu, C. J.; Fried, L. E. Ab Initio Study of RDX Decomposition Mechanisms. *J. Phys. Chem. A* **1997**, *101*, 8675−8679.
(23) Chakraborty, D.; Muller, R. P.; Dasgupta, S.; Goddard, W. A. The Mechanism for Unimolecular Decomposition of RDX (1,3,5-trinitro-1,3,5-triazine), an Ab Initio Study. *J. Phys. Chem. A* **2000**, *104*, 2261−2272.
(24) Chakraborty, D.; Muller, R. P.; Dasgupta, S.; Goddard, W. A. A Detailed Model for the Decomposition of Nitramines: RDX and HMX. *J. Comput.-Aided Mater.* **2002**, *8*, 203−212.
(25) Irikura, K. K.; Johnson, R. D. Is NO_3 Formed during the Decomposition of Nitramine Explosives? *J. Phys. Chem. A* **2006**, *110*, 13974−13978.
(26) Miao, M. S.; Dreger, Z. A.; Patterson, J. E.; Gupta, Y. A. Shock Wave Induced Decomposition of RDX: Quantum Chemistry Calculations. *J. Phys. Chem. A* **2008**, *112*, 7383−7390.
(27) Irikura, K. K. Aminoxyl (Nitroxyl) Radicals in the Early Decomposition of the Nitramine RDX. *J. Phys. Chem. A* **2013**, *117*, 2233−2241.
(28) Levine, R. D.; Bernstein, R. B. *Molecular Reaction Dynamics and Chemical Reactivity*; Oxford University Press: New York, 1987; p xii.
(29) Hase, W. L. Simulations of Gas-Phase Chemical-Reactions - Applications to S(N)2 Nucleophilic-Substitution. *Science* **1994**, *266*, 998−1002.
(30) Bowman, J. M.; Schatz, G. C. Theoretical-Studies of Polyatomic Bimolecular Reaction Dynamics. *Annu. Rev. Phys. Chem.* **1995**, *46*, 169−195.
(31) Zhao, Y.; Truhlar, D. G. A New Local Density Functional for Main-Group Thermochemistry, Transition Metal Bonding, Thermochemical Kinetics, and Noncovalent Interactions. *J. Chem. Phys.* **2006**, *125*, 194101.
(32) Fukui, K. The Path of Chemical Reactions - the IRC Approach. *Acc. Chem. Res.* **1981**, *14*, 363.
(33) Hratchian, H. P.; Schlegel, H. B. Accurate Reaction Paths Using a Hessian Based Predictor-Corrector Integrator. *J. Chem. Phys.* **2004**, *120*, 9918−9924.
(34) Hehre, W. J.; Ditchfield, R.; Pople, J. A. Self-Consistent Molecular-Orbital Methods. 12. Further Extensions of Gaussian-Type Basis Sets for Use in Molecular-Orbital Studies of Organic Molecules. *J. Chem. Phys.* **1972**, *56*, 2257−2261.
(35) Weigend, F. Accurate Coulomb-Fitting Basis Sets for H to Rn. *Phys. Chem. Chem. Phys.* **2006**, *8*, 1057−1065.
(36) Dunlap, B. I.; Rosch, N.; Trickey, S. B. Variational Fitting Methods for Electronic Structure Calculations. *Mol. Phys.* **2010**, *108*, 3167−3180.
(37) Frisch, M. J.; Trucks, G. W.; Schlegel, H. B.; Scuseria, G. E.; Robb, M. A.; Cheeseman, J. R.; Scalmani, G.; Barone, V.; Mennucci, B.; Petersson, G. A.; et al. *Guassian09, C.01*; Gaussian, Inc.: Wallington, CT, 2009.
(38) Seeger, R.; Pople, J. A. Self-Consistent Molecular-Orbital Methods. 18. Constraints and Stability in Hartree-Fock Theory. *J. Chem. Phys.* **1977**, *66*, 3045−3050.
(39) Bartlett, R. J. Coupled-Cluster Theory and Its Equation-of-Motion Extensions. *WIREs Comput. Mol. Sci.* **2012**, *2*, 126−138.
(40) Werner, H. J.; Knowles, P. J.; Knizia, G.; Manby, F. R.; Schutz, M. MOLPRO: a General-Purpose Quantum Chemistry Program Package. *WIREs Comput. Mol. Sci.* **2012**, *2*, 242−253.
(41) Dunning, T. H. Gaussian-Basis Sets for Use in Correlated Molecular Calculations. 1. The Atoms Boron through Neon and Hydrogen. *J. Chem. Phys.* **1989**, *90*, 1007−1023.
(42) Vladimiroff, T.; Rice, B. M. Reinvestigation of the Gas-Phase Structure of RDX Using Density Functional Theory Predictions of Electron-Scattering Intensities. *J. Phys. Chem. A* **2002**, *106*, 10437.
(43) Chapman, S.; Bunker, D. L. Exploratory Study of Reactant Vibrational Effects in $CH_3 + H_2$ and Its Isotopic Variants. *J. Chem. Phys.* **1975**, *62*, 2890−2899.
(44) Sloane, C. S.; Hase, W. L. Dynamics of State Selected Unimolecular Reactions - Chloroacetylene Dissociation and Predissociation. *J. Chem. Phys.* **1977**, *66*, 1523−1533.
(45) Schweigert, I. V.; Dunlap, B. I. Electronic Structure and Molecular Dynamics of Breaking the RO-NO_2 Bond. *J. Chem. Phys.* **2009**, *130*, 1523−1533.
(46) Kudin, K. N.; Scuseria, G. E.; Cances, E. A Black-Box Self-Consistent Field Convergence Algorithm: One Step Closer. *J. Chem. Phys.* **2002**, *116*, 8255−8261.

DOI: 10.1021/jp510034p
J. Phys. Chem. A 2015, 119, 2747−2759

(47) Bacskay, G. B. A. Quadratically Convergent Hartree-Fock (QC-SCF) Method - Application to Closed Shell Systems. *Chem. Phys.* **1981**, *61*, 385−404.
(48) Bacskay, G. B. A. Quadratically Convergent Hartree-Fock (QC-SCF) Method - Application to Open-Shell Orbital Optimization and Coupled Perturbed Hartree-Fock Calculations. *Chem. Phys.* **1982**, *65*, 383−396.
(49) Hratchian, H. P.; Schlegel, H. B. Using Hessian Updating to Increase the Efficiency of a Hessian Based Predictor-Corrector Reaction Path Following Method. *J. Chem. Theory Comput.* **2005**, *1*, 61−69.
(50) Grafenstein, J.; Kraka, E.; Filatov, M.; Cremer, D. Can Unrestricted Density-Functional Theory Describe Open Shell Singlet Biradicals? *Int. J. Mol. Sci.* **2002**, *3*, 360−394.
(51) Taube, A. G.; Bartlett, R. J. Improving upon CCSD(T): Lambda CCSD(T). I. Potential Energy Surfaces. *J. Chem. Phys.* **2008**, *128*, 044110.
(52) Rice, B. M.; Chabalowski, C. F. Ab Initio and Nonlocal Density Functional Study of 1,3,5-Trinitro-s-triazine (RDX) Conformers. *J. Phys. Chem. A* **1997**, *101*, 8720.
(53) Molt, R. W.; Watson, T.; Lotrich, V. F.; Bartlett, R. J. RDX Geometries, Excited States, and Revised Energy Ordering of Conformers via MP2 and CCSD(T) Methodologies: Insights into Decomposition Mechanism. *J. Phys. Chem. A* **2011**, *115*, 884−890.
(54) Bunker, D. L.; Hase, W. L. Non-RRKM Unimolecular Kinetics - Molecules in General, and CH_3NC in Particular. *J. Chem. Phys.* **1973**, *59*, 4621−4632.
(55) Tardy, D. C.; Rabinovitch, B. S. Intermolecular Vibrational Energy-Transfer in Thermal Unimolecular Systems. *Chem. Rev.* **1977**, *77*, 369−408.
(56) Klippenstein, S. J.; Harding, L. B.; Glarborg, P.; Gao, Y. D.; Hu, H. Z.; Marshall, P. Rate Constant and Branching Fraction for the NH_2 + NO_2 Reaction. *J. Phys. Chem. A* **2013**, *117*, 9011−9022.
(57) Hause, M. L.; Herath, N.; Zhu, R. S.; Lin, M. C.; Suits, A. G. Roaming-Mediated Isomerization in the Photodissociation of Nitrobenzene. *Nat. Chem.* **2011**, *3*, 932−937.
(58) Anderson, W. R.; Conner, C. B. Comparison of Gas-Phase Mechanisms Applied to RDX Combustion Model. *Proc. Combust. Inst* **2009**, *32*, 2123−2130.
(59) Glassman, I.; Yetter, R. A. *Combustion*, 4th ed.; Academic Press: Boston, 2008; p xx.
(60) Tarver, C. M.; Tran, T. D.; Whipple, R. E. Thermal Decomposition of Pentaerythritol Tetranitrate. *Propellants, Explos., Pyrotech.* **2003**, *28*, 189−193.
(61) Tarver, C. M.; Tran, T. D. Thermal Decomposition Models for HMX-Based Plastic Bonded Explosives. *Combust. Flame* **2004**, *137*, 50−62.
(62) Henson, B. F., Smilowitz, L. B. In *Shock Wave Science and Technology Reference Library Vol. 5: Non-Shock Initiation of Explosives*; Asay, B. W., Ed.; Springer-Verlag: Berlin, 2010; Chapter 3, pp 45−128.
(63) Baer, M. R. Modeling Heterogeneous Energetic Materials at the Mesoscale. *Thermochim. Acta* **2002**, *384*, 351−367.
(64) Henshaw, W. D.; Schwendeman, D. W. An Adaptive Numerical Scheme for High-Speed Reactive Flow on Overlapping Grids. *J. Comput. Phys.* **2003**, *191*, 420−447.
(65) Chinnayya, A.; Daniel, E.; Saurel, R. Modelling Detonation Waves in Heterogeneous Energetic Materials. *J. Comput. Phys.* **2004**, *196*, 490−538.
(66) Gonthier, K. A. Predictions for Weak Mechanical Ignition of Strain Hardened Granular Explosive. *J. Appl. Phys.* **2004**, *95*, 3482−3494.
(67) Anderson, W. R.; Meagher, N. E.; Vanderhoff, J. A. Dark Zones of Solid Propellant Flames: Critically Assessed Datasets, Quantitative Model Comparison, and Detailed Chemical Analysis. *Combust. Flame* **2011**, *158*, 1228−1244.
(68) Kumbhakarna, N.; Thynell, S. T.; Chowdhury, A.; Lin, P. Analysis of RDX-TAGzT Pseudo-Propellant Combustion with Detailed Chemical Kinetics. *Combust. Theory Modell.* **2011**, *15*, 933−956.
(69) Kapahi, A.; Udaykumar, H. S. Dynamics of Void Collapse in Shocked Energetic Materials: Physics of Void-Void Interactions. *Shock Waves* **2013**, *23*, 537−558.
(70) Barua, A.; Kim, S.; Horie, Y.; Zhou, M. Ignition Criterion for Heterogeneous Energetic Materials Based on Hotspot Size-Temperature Threshold. *J. Appl. Phys.* **2013**, *113*, 064906.
(71) Brennan, J. K.; Lisal, M.; Moore, J. D.; Izvekov, S.; Schweigert, I. V.; Larentzos, J. P. Coarse-Grain Model Simulations of Non-equilibrium Dynamics in Heterogeneous Materials. *J. Phys. Chem. Lett.* **2014**, *5*, 2144−2149.

DOI: 10.1021/jp510034p
J. Phys. Chem. A 2015, 119, 2747−2759